Numerical Simulation of Cold Flow in an Axisymmetric Centerbody Combustor

J. N. Scott*
University of Dayton Research Institute, Dayton, Ohio
and
W. L. Hankey Jr.†
Air Force Wright Aeronautical Laboratories, Wright-Patterson Air Force Base, Ohio

The unsteady compressible Navier-Stokes equations are solved numerically for cold flow in an axisymmetric bluff centerbody combustor configuration. The inlet Mach number range in the annulus is 0.145-0.387, which corresponds to inlet mass flows of about 2-4 kg/s and a Reynolds number ($Re_D = u_\infty D/\nu$) range of 0.37-1.1 × 10⁶. The computations are performed using MacCormack's explicit finite difference scheme on a CDC Cyber 750/175 computer. The computational mesh consists of 2760 grid points. As a result of the low subsonic flow velocity, special care is required in formulating the inflow and outflow boundary conditions necessary to obtain valid numerical solutions. The resulting oscillatory flowfields show some qualitative agreement with experimental observations. The vortex behavior is of particular interest in the centerbody region since it influences the mixing of fuel from the central jet and the flow from the annulus and, consequently, the combustion itself.

Nomenclature

c	= speed of sound
D	= diameter of centerbody
e	= specific energy
E,F	= vector fluxes in mean flow equations
f	= frequency
H	= source term
i,j	= indices for grid point location
k	= thermal conductivity
L	= length of computational domain
n	= time index
p	= pressure
r	= radial coordinate
R	= gas constant
R_{CB}	= radius of centerbody
S_t	= Strouhal number
t	= time
T	= temperature
TCH	= characteristic time, L/u_∞
u,v	= velocity components
U	= dependent variable
x	= axial coordinate
β	= damping factor
γ	= ratio of specific heats
η,ζ	= transformed coordinates
λ	= $-\frac{2}{3}\mu$ second viscosity coefficient
μ	= molecular viscosity coefficient
ρ	= density
σ_x,σ_r	= normal stresses
τ_x,τ_r	= shear stresses
ω	= vorticity

Subscripts

∞	= freestream condition (annulus velocity)
JL_{max}	= maximum value
KL_{min}	= minimum value
$t0$	= stagnation values
w	= wall condition

Presented as Paper 83-1741 at the AIAA 16th Fluid and Plasma Dynamics Conference, Danvers, Mass., July 12-14, 1983; received Aug. 9, 1983; revision received April 4, 1984. This paper is declared a work of the U.S. Government and therefore is in the public domain.

*Research Engineer, Aerospace Mechanics Division. Member AIAA.
†Senior Scientist. Associate Fellow AIAA.

Introduction

THE evolution of advanced high-speed aircraft has led to requirements for improved design methodology for propulsion systems. In order to meet these requirements, improved combustion models are being investigated for possible application to advanced propulsion system technology. The development of improved combustion models requires a thorough understanding of the interaction between the flowfield and the combustion process. To aid in the development and evaluation of new combustion models, a research combustor facility has been developed in the Aero Propulsion Laboratory at Wright-Patterson Air Force Base for the purpose of conducting experimental investigations. This facility consists of a cylindrical bluff centerbody placed coaxially in a circular duct. The test section is shown schematically in Fig. 1. As seen in the figure, fuel enters through a small opening in the base of the bluff centerbody. The combustion takes place immediately downstream of the centerbody in the wake or recirculation region. In the initial evaluation of this facility, unsteady flame behavior was observed in the recirculation region through high-speed ciné photography. Experimental investigations of this unsteady flame behavior[1-3] provided the motivation for the current numerical study.

The objective of this numerical simulation is to investigate the feasibility of analyzing unsteady flow features by numerically solving the time-dependent Navier-Stokes equations and to gain a better insight into the nature of specific unsteady flow features in the combustor recirculation region. Of particular interest here is the shedding of large-scale vortices, since this phenomenon appears to contribute significantly to the mixing of fuel and air and ultimately to the combustion process itself. The flow over the bluff body results in separated flow, which has an inflection point in the velocity profile. Such separated flows typically possess a relatively low natural frequency at which self-excited oscillations occur.[4-9] The vortex shedding from the buff

centerbody exhibits the characteristics of self-excited oscillations.

In the past only steady flow calculations have been used to numerically investigate recirculating flows.[10,11] In the present investigation, the full time-dependent Navier-Stokes formulation[4-9] is utilized to numerically simulate the unsteady axisymmetric internal flowfield. In performing these calculations, the vortex shedding, vortex pairing, and annihilation have been numerically simulated for the first time. These computed flowfields will be used to analyze specific features in the vortex behavior including (Strouhal) shedding, separation and reattachment points or nodes in the flowfield, stagnation points, and the pairing and merging of vortices. Analysis of these features will provide a better insight into the nature of the unsteady flow phenomena and how they contribute to the combustion process. The combustion process itself depends upon the mixing of the outer annulus airflow and the fuel flow from the centerbody jet flow.[1] The present investigation is the first phase, which deals only with the cold flow from the outer annulus.

Analysis

Based on experimental data from the bluff-body combustor facility, consisting of high-speed ciné photographs and flame intensity measurements, the flow appears to be generally axisymmetric a large fraction of the time.[3] Therefore, in this preliminary investigation the axisymmetric assumption will be used to gain insight into the flow phenomena. Thus, numerical solution of the time-dependent Navier-Stokes equations is used to simulate the flow.

The computer code used in this investigation is based on a program developed by Shang[5,6,12] for solving the time-dependent, compressible Navier-Stokes equations. The governing equations are written in cylindrical polar coordinates as

$$\boldsymbol{U}_t + \boldsymbol{E}_x + (1/r)(rF)_r = \boldsymbol{H} \tag{1}$$

where

$$\boldsymbol{U} = \begin{bmatrix} \rho \\ \rho u \\ \rho v \\ \rho e \end{bmatrix} \tag{2}$$

$$\boldsymbol{E} = \begin{bmatrix} \rho u \\ \rho u^2 - \sigma_{xx} \\ \rho uv - \tau_{rx} \\ \rho ue - u\sigma_{xx} - v\tau_{xr} - kT_x \end{bmatrix} \tag{3}$$

$$\boldsymbol{F} = \begin{bmatrix} \rho v \\ \rho uv - \tau_{rx} \\ \rho v^2 - \sigma_{rr} \\ \rho ve - v\sigma_{rr} - u\tau_{xr} - kT_r \end{bmatrix} \tag{4}$$

$$\boldsymbol{H} = \begin{bmatrix} 0 \\ 0 \\ -\tau_{\theta\theta}/r \\ 0 \end{bmatrix} \tag{5}$$

and where the components of the stress tensor are given by

$$\sigma_{xx} = (2\mu + \lambda)\frac{\partial u}{\partial x} + \lambda\left(\frac{v}{r} + \frac{\partial v}{\partial r}\right) - p \tag{6}$$

$$\sigma_{rr} = (2\mu + \lambda)\frac{\partial v}{\partial r} + \lambda\left(\frac{v}{r} + \frac{\partial u}{\partial x}\right) - p \tag{7}$$

$$\tau_{\theta\theta} = (2\mu + \lambda)\frac{v}{r} + \lambda\left(\frac{\partial u}{\partial x} + \frac{v}{r}\right) - p \tag{8}$$

$$\tau_{xr} = \tau_{rx} = \mu\left(\frac{\partial u}{\partial r} + \frac{\partial v}{\partial x}\right) \tag{9}$$

The dependent variables for this system of equations are $U(\rho, \rho u, \rho v, \rho e)$. Sutherland's viscosity equation, the equation of state, and the Prandtl number are specified to close this system of equations.

For the present investigation, this code has been modified so that the no-slip boundary conditions are applied at the outer duct wall and around the centerbody surface and a symmetry boundary condition is applied at the duct centerline.

Treatment of the inflow and outflow conditions are among the primary focuses of this investigation. Hence, the computations are made using the inflow and outflow conditions studied by Hasen using a similar code.[13] These conditions consist of the following:

Inflow: P_{t0}, T_{t0}, $v = 0$ specified

$$\frac{\partial(\rho u)}{\partial x} = 0 \tag{10}$$

Outflow:

$$\frac{\partial u}{\partial x} = \frac{\partial v}{\partial x} = \frac{\partial T}{\partial x} = 0 \tag{11}$$

P specified (inviscid region),

$$\frac{\partial P}{\partial x} = 0 \text{ (viscous region)}$$

These conditions are shown in Fig. 2. For Hasen's code, these conditions allowed the numerical flow variables in the combustor domain to remain stable during the computation. It should be noted here that several other formulations of the boundary conditions have been attempted without success and that there may indeed be other formulations[14] which will permit successful computations of the flowfield using the present code. While the present boundary conditions give successful results, additional formulations should be investigated, including the location of the downstream boundary condition that is applied at five centerbody radii downstream in the present case. It is downstream of the stagnation point; however, additional studies should be made.

Computational Grid System

The physical finite difference mesh used in the numerical solution of the combustor flowfield is shown in Fig. 3. An axisymmetric flow assumption is made in the formulation, with the mesh extending radially from the centerline to the

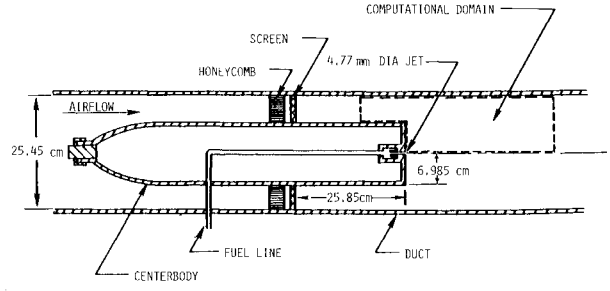

Fig. 1 Aero Propulsion Laboratory's centerbody combustor configuration.

duct wall. An exponential stretching scheme is utilized in both the axial and radial directions in order to position a fine mesh near the walls of the duct and centerbody and in the recirculation zone in the near wake of the centerbody. This permits better resolution of the flowfield in the regions of high gradients. (Although a fuel jet can be included in the procedure, the case presented here has no central fuel jet in the centerbody.) The number of mesh points used in the numerical solution consists of 60 points in the axial direction and 46 points radially.

Numerical Procedure and Solution Scheme

The flowfield being investigated in this program is in the low subsonic region. Experimental observations have revealed the presence of unsteady phenomena having an apparent quasiperiodic nature.[1,3] Preliminary indications suggest that a Strouhal number for the phenomena would fall within a range of 0.18-0.22. This would correspond to a vortex shedding frequency of about 70 Hz. The characteristic time L/u_∞ is 5.2×10^{-3} s for the present analysis.

In view of the previous work by Shang[5,12] and Hankey and Shang,[6] the code selected for this application incorporates MacCormack's explicit and unsplit algorithm as the numerical solution procedure. This code has been optimized for vector operation to minimize the number of sweeps over the entire data field. Furthermore, the axisymmetric formulation allows for the coordinate transformation derivatives to be computed once and stored before proceeding into the time marching.

MacCormack's algorithm involves a combination of alternating forward and backward differences for the predictor and corrector steps.[15] It should be noted, however, that the source-like term $\tau_{\theta\theta}/r$ in the $\boldsymbol{H}$ vector (that is, in the radial momentum equation) is evaluated using a central differencing procedure. In addition, the term contained in the radial gradient operator $1/r\cdot\partial/\partial r(rv)$ is further expanded giving the expressions $\partial v/\partial r$ and v/r. This alleviates the numerical difficulty encountered when an indeterminate form arises on the axis of the symmetry. Grid stretching is required in order to resolve the flowfield features more adequately while maintaining computational efficiency.

To achieve this capability, Eq. (1) is transformed to a computational domain with equal step size. Due to the simplicity of the geometry of the combustor, only a minor transformation is required. Letting

$$\zeta=\zeta(x) \quad \text{and} \quad \eta=\eta(r)$$

Eq. (1) is transformed as follows:

$$U_t+\zeta_x E_\zeta+(\eta_r/r)\,(rF)_\eta=H \tag{12}$$

This is consistent with the general procedure for surface-oriented coordinate systems currently in use in computational fluid dynamics.

The efficiency of the code is maximized utilizing the CFL condition on allowable time increment for generalized coordinates as reported by Shang,[12]

$$\Delta t_{\mathrm{CFL}}=\left\{\frac{\bar u}{\Delta\eta}+\frac{\bar v}{\Delta\zeta}+c\left[\left(\frac{\eta_x}{\Delta\eta}+\frac{\zeta_x}{\Delta\zeta}\right)^2+\left(\frac{\eta_y}{\Delta\eta}+\frac{\zeta_y}{\Delta\zeta}\right)^2\right]^{1/2}\right\}^{-1} \tag{13}$$

with the contravariant velocity components defined as

$$\bar u=\zeta_x u+\zeta_r v \tag{14}$$

$$\bar v=\eta_x u+\eta_r v \tag{15}$$

The range of CFL numbers used in the present investigation vary from 0.15 to as high as 0.85. Although most of the calculations have been made using a CFL number of 0.5, this value seems to provide stable results in a reasonable computational time.

The numerical damping is also used in the present analysis in order to suppress numerical oscillations. Again the form of the damping terms is reported by Shang.[12] Implemented in each sweep direction, these damping or artificial viscosity terms are

$$\beta\Delta t\Delta\eta^3\{|\bar u|+(\eta_x^2+\eta_y^2)^{1/2}c\}\frac{1}{p}\left|\frac{\partial^2 p}{\partial\eta^2}\right| \tag{16}$$

$$\beta\Delta t\Delta\zeta^3\{|\bar v|+(\zeta_x^2+\zeta_y^2)^{1/2}c\}\frac{1}{p}\left|\frac{\partial^2 p}{\partial\zeta^2}\right| \tag{17}$$

In the present analysis, the value of the damping constant β is two.

In the analysis of self-excited oscillations, the large-scale turbulence is computed from first principles by a large-eddy simulation; however, the fine-scale turbulence is masked by the artificial viscosity. The maximum frequency resolved in the problem is equal to $u_\infty/\Delta x$ ($\sim$3000 Hz). A large portion of the turbulent energy is believed to be below this frequency; therefore, reasonable simulation is achieved.[4,6]

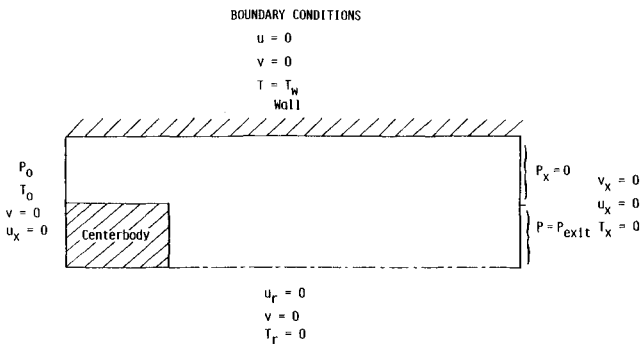

Fig. 2 Boundary conditions.

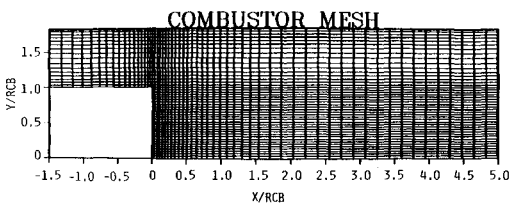

Fig. 3 Physical finite difference mesh used in the numerical solution of the combustor flowfield.

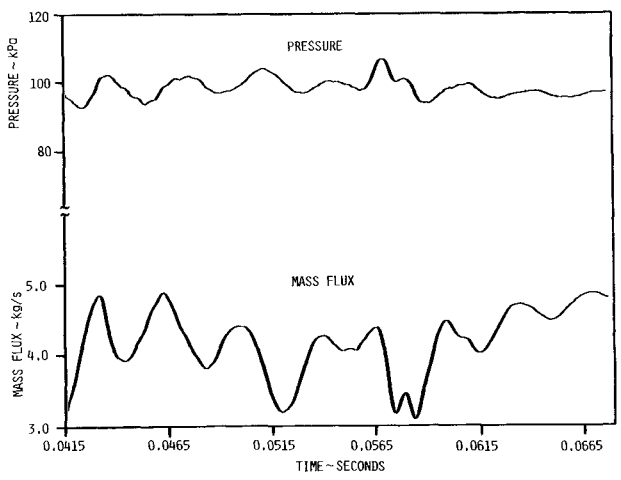

Fig. 4 Temporal variation of the inflow mass flux and pressure at $x/\mathrm{RCB}=1$, $r/\mathrm{RCB}=1$.

Discussion of Results

In the present combustor configuration, only airflow in the annulus is considered with no central jet present. For this configuration, computations have been carried out for 25,700 time steps. This represents approximately 68 ms of real time in the flow. The nature of the flow is indicated by the temporal variation of the inflow mass flux and pressure at a location of one centerbody radius downstream as shown in Fig. 4. During the initial computations ($u_\infty \sim 50$ m/s), the fluctuations occurred at a frequency of about 70 Hz. This agrees well with experimental wall pressure data[16] (not yet published) that, for the same airflow rate, contains a fluctuation at about the same frequency (70 Hz). These experimental data were obtained from the Aero Propulsion Laboratory centerbody combustor facility with cold flow and the same initial conditions as the numerical simulation. This frequency corresponds to a classical Strouhal shedding for which the Strouhal number is

$$S_t = fD/u \approx 0.2 \tag{18}$$

where f is the frequency, D the centerbody diameter, and u the mean annulus inflow velocity. This value of Strouhal number agrees well with values observed for vortex shedding from other objects such as cylinders (i.e., $S_t \sim 0.2$).[5,6,8,9]

Certain similarities between the computed vortex behavior behind the bluff centerbody and experimental observations are extremely encouraging for this type of numerical approach. The computed results for instantaneous velocity vector fields are shown in Fig. 5 for a sequence of time steps; Fig. 6 shows vorticity contours for some of these same time steps. Examination of the velocity vector plots reveals the development of a large primary recirculating vortex having a clockwise rotation immediately downstream of the cen-

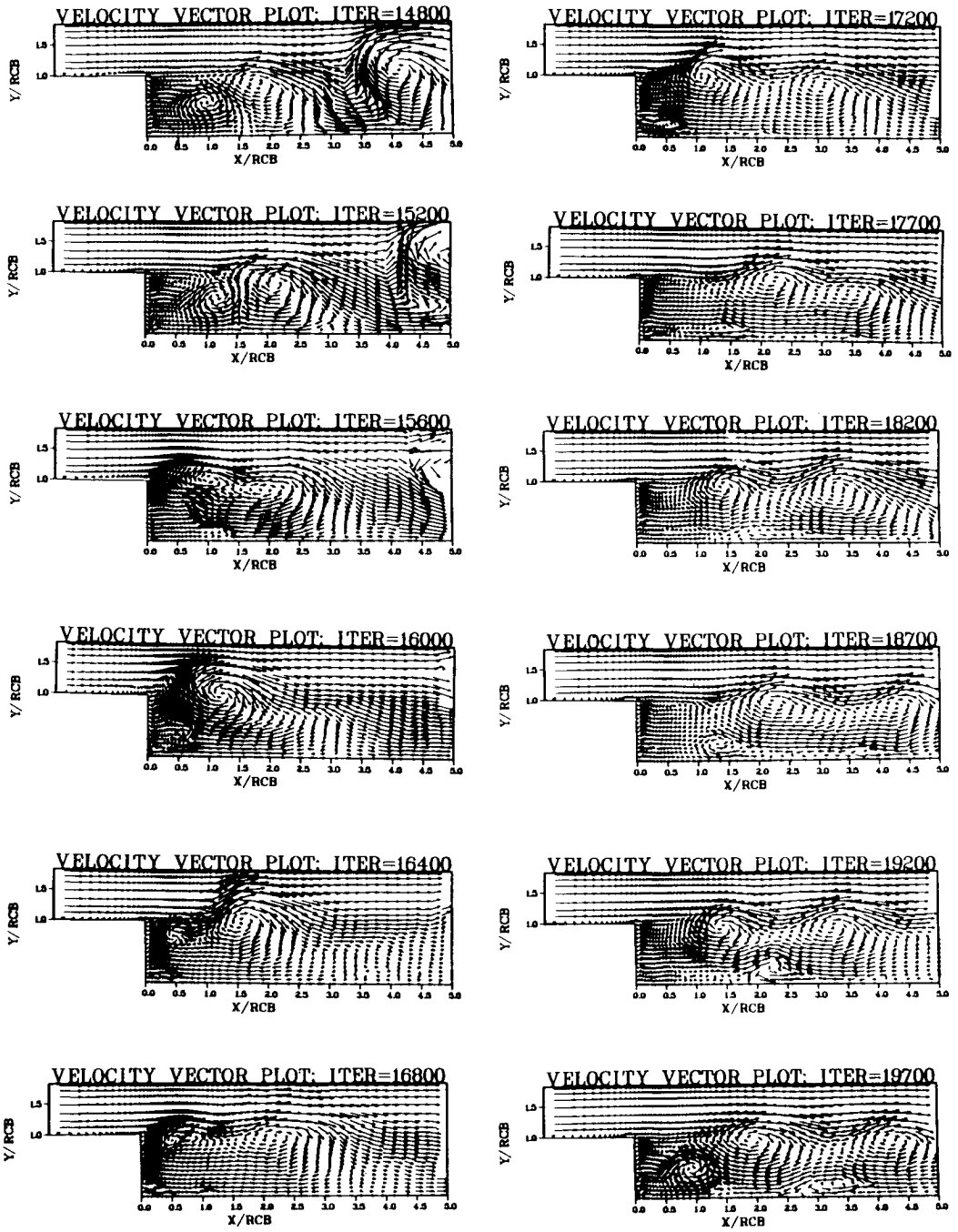

Fig. 5a Velocity vectors, 1 ITER = 3×10^{-6} s.

terbody. This recirculating vortex induces a counterrotating (counterclockwise) vortex near the axis of the bluff body. This induced vortex behavior occurs in accordance with the classic Biot-Savart law.[17] This counterrotating vortex may either grow in strength or die out, or merge with the recirculating vortex as it progresses in the streamwise direction. If it gains sufficient strength (as in ITER = 19700-ITER = 21700), it pushes the initial recirculating vortex downstream. As it does so, a new recirculating vortex is generated which induces a new counterrotating vortex. If the counterrotating vortex is weak, the two adjacent clockwise recirculating vortices may merge, thus annihilating it, or it may decay along the centerline. These phenomena are observed in sequences labeled ITER = 14800-ITER = 16000 and ITER = 17200-ITER = 18200, respectively.

Another phenomenon observed is that of "vortex leapfrogging." This is a situation in which the leading vortex ring decelerates and at the same time decreases in diameter, while the trailing vortex (of the same rotational sense, namely clockwise) accelerates and increases in diameter to overtake the leading vortex. This is seen in the vorticity contours of ITER = 17200-ITER = 18200. In this case, the two vortices involved in the leapfrogging were initially the large recirculating vortices. The induced counterrotating vortex between them is very weak and has decayed along the centerline. This type of leapfrogging of vortex rings is analogous to that described for free jet flows by Lamb,[18] and Prandtl, and Tietjens.[19] (It should be noted that these computed flows contain similarities with features observed in combusting flow behind a two-dimensional rearward-facing step in experiments conducted by Keller et al.[20]) These figures show the general oscillatory nature of the vortex shedding and the subsequent pairing or merging of the vortices. A careful examination of the velocity vectors and vorticity contours

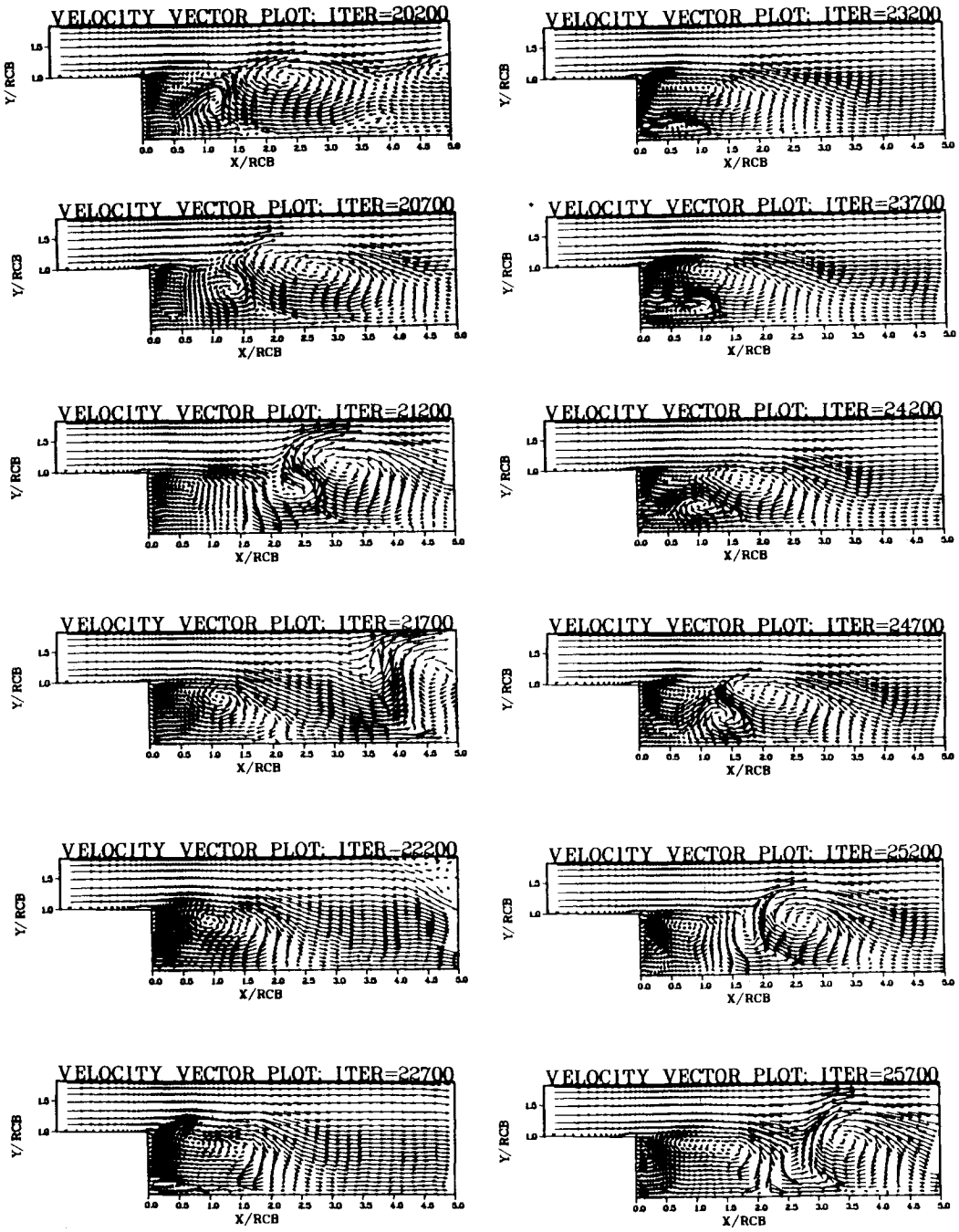

Fig. 5b Velocity vectors, 1 ITER = 3×10^{-6} s.

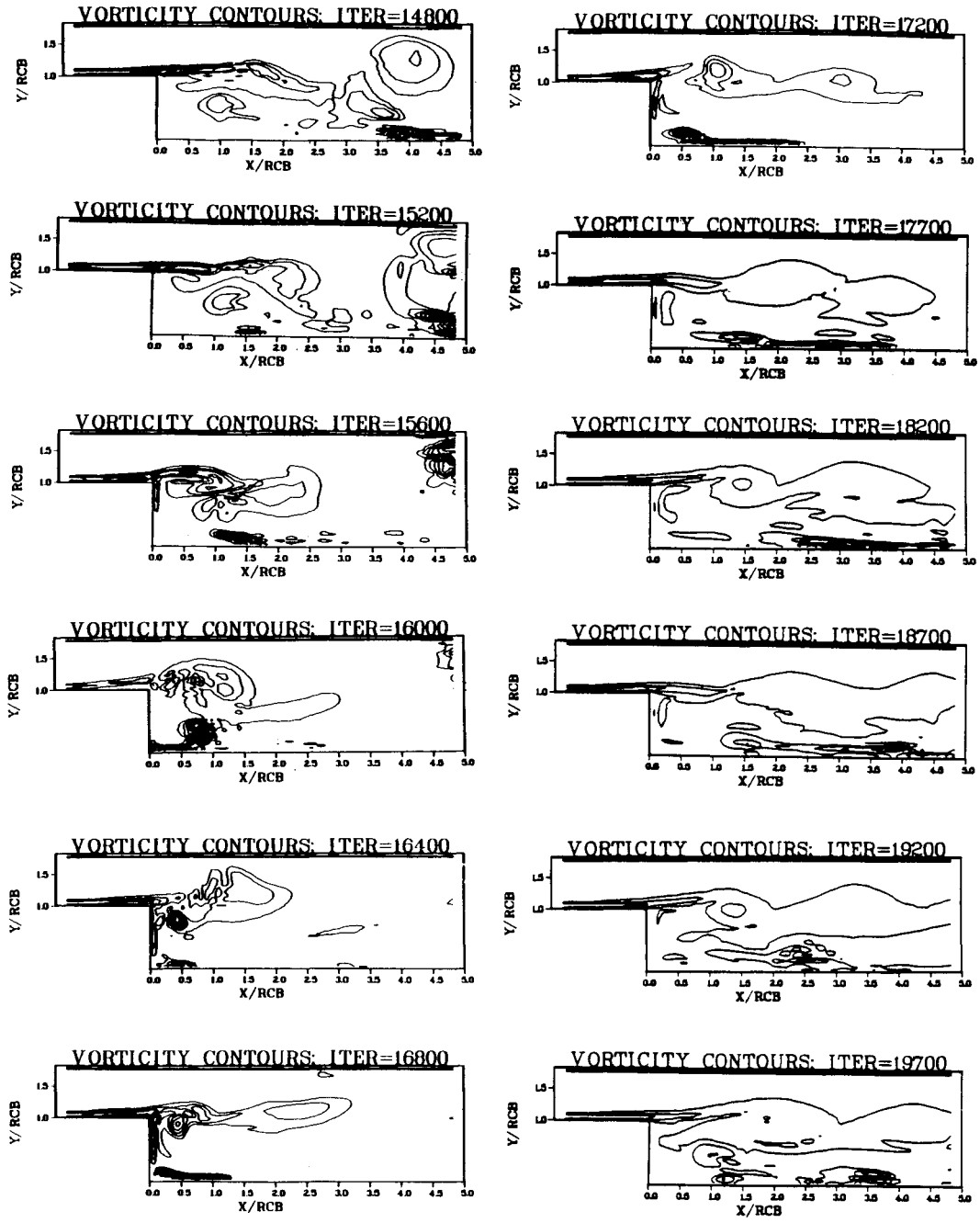

Fig. 6 Vorticity contours.

(Figs. 5 and 6) show the primary vortex shedding from the outer portion of the bluff-body face at a frequency of about 70 Hz. This is supported by the periodic fluctuation of the mass flux and pressure (Fig. 4).

It should be noted that the formation and shedding of the secondary counterrotating vortices does not occur at exactly the same frequency as the primary "outer" vortices. The shedding of both the primary and secondary vortices exhibit the characteristics of self-excited oscillations. It must be further mentioned that this sequence of events does not occur in exactly the same fashion with each cycle. In particular, instances have been observed in the numerical results in which more than two vortices merge into a single vortex. The fact that a completely repeatable periodic behavior is not observed is believed to be the result of multiple modes being present. Two unstable modes, with differing noncommensurable frequencies, will produce a nonrepeating wave. The most unstable wave will dominate with a modulation created by the lower amplitude wave. The numerical procedure apparently captures both modes. The phenomena of more than two vortices merging has been observed experimentally by Ho and Huang[21] and is referred to as collective interaction.

The streamwise paths of the computed vortices with time are shown in the wave diagram of Fig. 7. This figure shows not only the streamwise trajectories of the vortex centers, but the pairing of vortices as well. Along with the locations at which pairing occurs, it can be seen from this figure that occasionally more than two vortices merge to form a single vortex. It is seen that the trajectory lines are nearly parallel to each other, thus indicating that the vortices are convected in the streamwise direction at nearly the same speed. This propagation speed is approximately half of the flow velocity, which is consistent with linear theory.[4]

Another feature of significance in Figs. 5 and 6 and especially in Fig. 4 is a second periodic variation having a frequency of about 300 Hz. This is believed to be associated

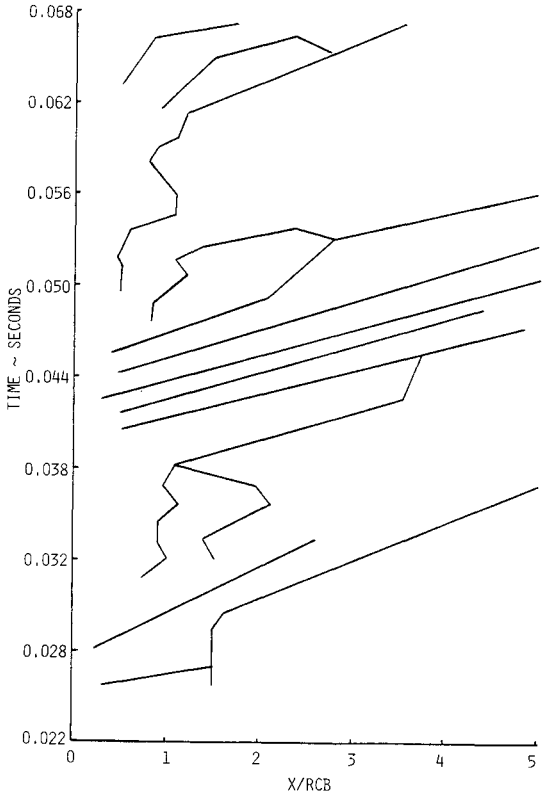

Fig. 7 Vorticity wave diagram.

with the natural acoustic frequency based on the "computational" duct length,[4] that is, the natural acoustic frequency of a duct of the same length as the computational domain.

In view of the complex nature of the flow over the bluff body, one of the best ways to gain a better understanding of the specific features associated with it is through direct flow visualization. This can be simulated by plotting the vorticity contour data on a color graphics device using continuous color shading between the contours. A sequence of color vorticity plots is shown in Fig. 8. In this figure the vortex formation, shedding, and pairing can be seen once again. By presenting the data in this form, similarities between the numerical results and certain aspects of the combusting flow can be noted. It must be emphasized that the present numerical simulation does not completely model the combustion experiment, since the computational configuration does not include the flow from the central jet, combustion, nor identical airflow rate. Furthermore, the length of the computational domain is restricted to only a fraction of the actual combustor length. In spite of these differences, the numerical simulation of certain features of the combustor flow is very encouraging. In comparing the color vorticity plots with the high-speed ciné photographs of the combustion data, the similarities in the large recirculation vortex near the outer edge of the centerbody face are seen. This vortex then stretches in the streamwise direction and is ultimately shed and propagates downstream. It appears that the flame balls or "flame turbules" observed in the combustor are directly related to the vortex shedding. Comparison of specific flow features between the cold-flow simulation and the actual combustor flow is even more dramatic in a movie made using the numerical vorticity data. (Unfortunately, the comparison of these dynamic features cannot be shown here.)

Although some of these similarities are quite striking, caution must be exercised in examining the numerical vorticity data because certain features may not truly represent the physical combustion flow. The flow must be examined more closely, using quantitative comparisons, in order to accurately determine the nature of the actual physical flow.

Other features giving insight into the nature of the flow are singular points that are present on boundaries such as the centerline and the centerbody face. It is noted that on the centerline, points occur at which the flow approaches from opposite directions along the centerline and departs in a direction nearly normal to the centerline. Likewise, points exist on the centerline where the flow approaches from a direction nearly normal to the centerline and departs in opposite directions along the centerline. These points exhibit the characteristics of classical saddle points and are somewhat analogous to the separation and reattachment points that occur at solid boundaries. The saddle points on the centerline have been designed as S and R points in Fig. 9, depending upon the nature of the entering and departing flow. These points move in the streamwise direction at a rate closely related to the convection velocity of the vortices. The initial separation between the S and R points is almost three radii, which corresponds to the vortex separation distance.

On the centerbody face (a solid boundary), the presence of separation (S) and reattachment (R) points is also indicated in Fig. 9. It is noted that a stationary separation point is always present at the outside edge of the centerbody face, while the corresponding reattachment point may move along the radial direction of the centerbody face. Of particular note is the presence of a stationary separation point at the upper corner of the centerbody (S_1). A separation streamline starts at this point and evolves into a vortex. An adjacent streamline appears to act as a sort of boundary for the large recirculation vortex that forms on the centerline (R_2). The reattachment position of this line transverses along the centerline as the clockwise recirculation vortices are shed.

Similarly a reattachment point (R_1) occurs on the face of the centerbody. This reattaching streamline separates the counterrotating (i.e., counterclockwise) vortex B from the clockwise recirculation vortex A. The location of the reattachment point on the centerbody face varies with the growth and ultimate shedding of the counterclockwise vortex. Likewise, the corresponding saddle point (S_2) moves along the centerline according to the behavior of the counterclockwise vortex.

One significant aspect of the behavior of the reattachment point on the centerbody face is that it moves no further outward than about three-fourths of a radius from the centerline. To the outside of this point, the flow is always in the outward radial direction along the centerbody face. During a large percentage of the time, the magnitude of the velocity in this region is very small. That is, this is a zone of nearly stagnant fluid.

As the vortices form and propagate downstream, the interaction between adjacent vortices varies depending on the sense of rotation and the relative strength of each vortex. In most cases, it is observed that the centers of two counterrotating vortices tend to rotate about one another. The rotation of these vortex centers is in the clockwise sense when the leading vortex rotates in the clockwise direction. In the course of this rotation, two clockwise vortices on either side of the counterclockwise vortex merge into one clockwise vortex, while annihilating the counterclockwise vortex (Fig. 5). The interactions observed between adjacent vortices shed from the outer edge of the centerbody, having clockwise rotation, are seen in Fig. 5 from ITER = 17400 to about ITER = 20000. In this case the induced vortex near the centerline is relatively weak. When this happens, the classical vortex "braiding" occurs.[22] For this type of interaction, a saddle point exists between the two vortices. The behavior of these two vortices is of great significance[1] in analyzing the combustor in that the counterclockwise vortex contains the fuel, while the clockwise vortex contains the oxidizer.

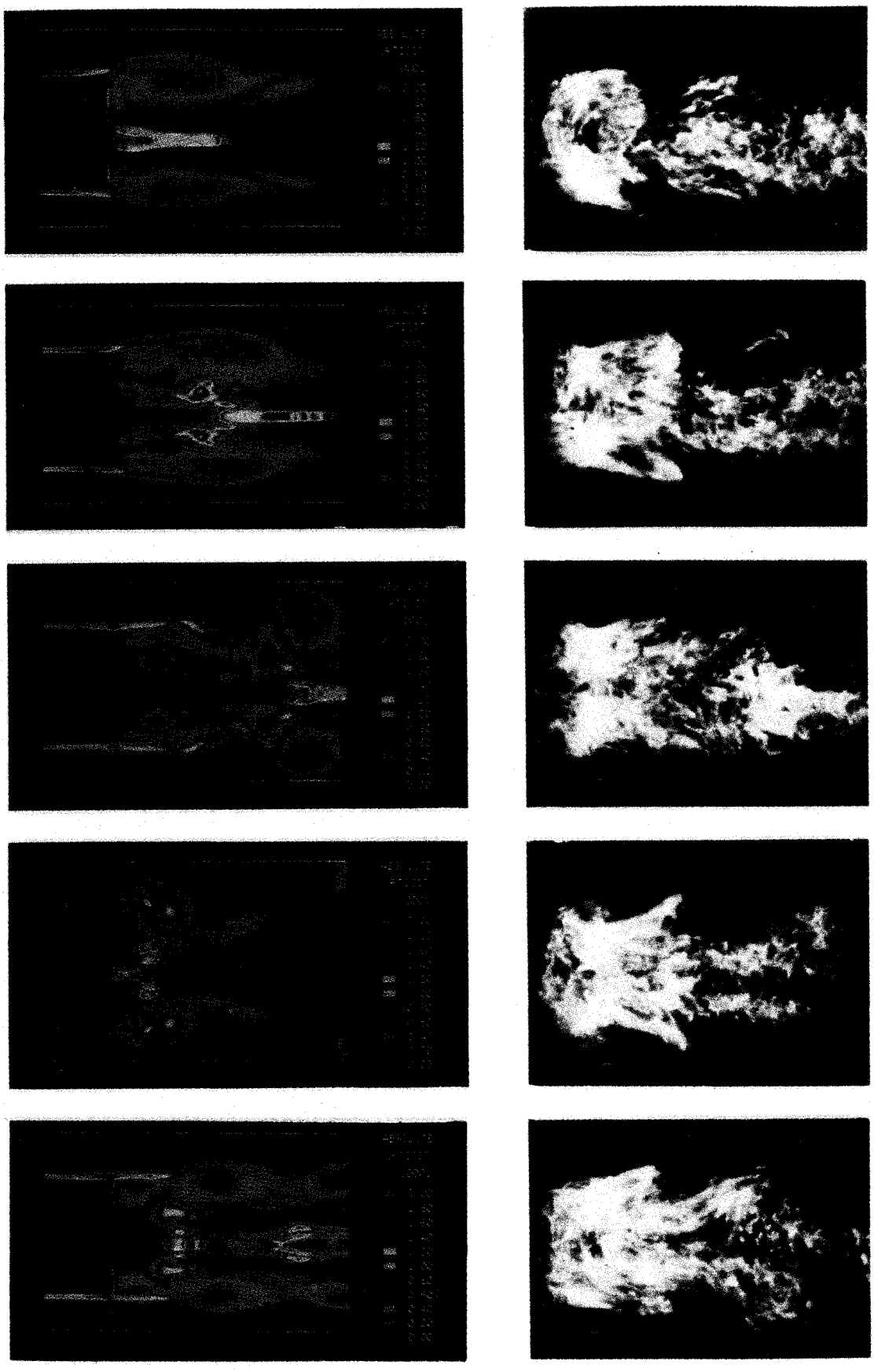

Fig. 8 Comparison of computed flowfield vorticity with experimental combustor flow features.

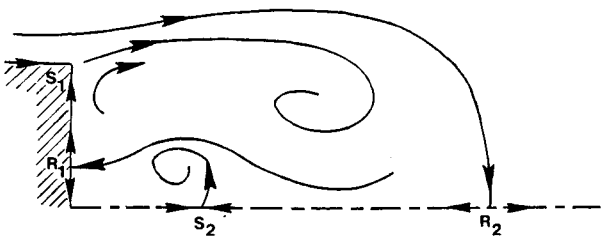

Fig. 9 Typical S and R saddle points.

The merging of these two vortices as demonstrated in the numerical computation is essential to the combustion process. The stage is now set for the addition of the fuel jet with a chemical reaction to complete the modeling of a centerbody combustor.

Conclusions

The unsteady fluid dynamic processes that occur in this type of flow configuration can be predicted only by the numerical integration of time-dependent Navier-Stokes equations. As the first phase of a numerical computation of flow in a combustor, this paper demonstrates the feasibility of modeling the self-excited oscillation involved in vortex shedding in axisymmetric flow. It should be emphasized that the computed results are for cold flow only and that certain questions remain unanswered concerning the formulation of the boundary conditions. Although these numerical results are preliminary in nature, they will provide insight into the mixing process when used in conjunction with the experiments and can help guide further research in the combustion field. Now the fuel jet with chemical reaction can be added to the computer program to more thoroughly investigate the unsteady combustion process.

Acknowledgment

This work of the first author was conducted under Contract F33615-82-K-2252 with the Aero Propulsion Laboratory/AFWAL, Wright-Patterson Air Force Base, Ohio. The work was funded by AFOSR under Aero Propulsion Laboratory Work Unit 23085705. The authors would like to thank the Air Force Technical Monitor, Dr. W. M. Roquemore, for his cooperation and support and in particular for providing the high-speed ciné films of the experimental flowfield. We would also like to express our appreciation to Drs. J. S. Shang and G. H. Hasen for many fruitful discussions and suggestions throughout the course of the investigation, and to Dr. Hasen and Mr. M. F. Maglich for providing the color graphics outputs, including the movie.

References

[1] Roquemore, W. M., Britton, R. L., and Sandhu, S. S., "Investigation of the Dynamic Behavior of a Bluff Body Diffusion Using Flame Emission," AIAA Paper 82-0178, Jan. 1982.

[2] Lightman, A. J. and Magill, P. D., "Velocity Measurements in Confined Dual Coaxial Jets Behind an Axisymmetric Bluff Body: Isothermal and Combusting Flows," AFWAL-TR-82-2018, April 1981.

[3] Roquemore, W. M., Bradlen, R. P., Stutrud, J. S., Reeves, C. M., and Britton, R. L., "Influence of the Vortex Shedding Process on a Bluff-Body Diffusion Flame," AIAA Paper 83-0335, Jan. 1983.

[4] Hankey, W. L. and Shang, J. S., "Analysis of Self-Excited Oscillations in Fluid Flows," AIAA Paper 80-1346, July 1980.

[5] Shang, J. S., "Oscillatory Compressible Flow Around a Cylinder," AIAA Paper 82-0098, Jan. 1982.

[6] Hankey, W. L. and Shang, J. S., "Natural Transition-A Self-Excited Oscillation," AIAA Paper 82-1011, June 1982.

[7] Newsome, R. W., "Numerical Simulation of Near Critical and Unsteady Subcritical Inlet Flow Field," AIAA Paper 83-0175, Jan. 1983.

[8] Hankey, W. L. and Shang, J. S., "The Numerical Solution of Pressure Oscillations in an Open Cavity," AIAA Paper 79-0136, Jan. 1979.

[9] Shang, J. S., Smith, R. E., and Hankey, W. L., "Flow Oscillations of Spike Tipped Bodies," AIAA Paper 80-0062, Jan. 1980.

[10] Sturgess, G. J. and Syed, S. A., "Dynamic Behavior of Turbulent Flow in a Widely-Spaced Co-Axial Jet Diffusion Flame Combustor," AIAA Paper 83-0575, Jan. 1983.

[11] Krishnamurthy, L., "Isothermal Flowfield Predictions of Confined Coflowing Turbulent Jets in an Axisymmetric Bluff-Body Near Wake," AFWAL-TR-81-2036, May 1981.

[12] Shang, J. S., "Numerical Simulation of Wing-Fuselage Aerodynamic Interaction," AIAA Paper 83-0225, Jan. 1983.

[13] Hasen, G., "A Navier-Stokes Solution for Cold Flow in an Axisymmetric Combustor," AFWAL-TM-82-171-FIMM, March 1982.

[14] Oliger, J., "On the Initial Boundary Value Problem for the Equations of Gas Dynamics," *Transactions of the Twenty-fifth Conference of Army Mathematicians*, ARO Rept. 80-1, 1980, pp. 417-425.

[15] MacCormack,. R. W., "Numerical Solution of the Interaction of a Shock Wave with a Laminar Boundary Layer," *Lecture Notes in Physics*, Vol. 59, Springer-Verlag, New York, 1971, p. 151.

[16] Roquemore, W. M., Personal communication, 1983.

[17] Rockwell, D. and Naudascher, E., "Self-Sustained Oscillations of Impinging Free Shear Layers," *Annual Review of Fluid Mechanics*, 1979, pp. 67-94.

[18] Lamb, H., *Hydrodynamics*, 6th ed., Dover Publications, New York, 1945, p. 242.

[19] Tietjens, O. G., *Fundamentals of Hydro- and Aeromechanics*, Dover Publications, New York, 1957 (United Engineering Trustees, Inc., 1934), p. 212.

[20] Keller, J. O. et al., "Mechanism of Instabilities in Turbulent Combustion Leading to Flashback," *AIAA Journal*, Vol. 20, Feb. 1982, pp. 254-262.

[21] Ho, C. and Huang, L., "Subharmonics and Vortex Merging in Mixing Layers," *Journal of Fluid Mechanics*, Vol. 119, 1982, pp. 443-473.

[22] Broadwell, J. E. and Breidenthal, R. E., "A Simple Model of Mixing and Chemical Reaction in a Turbulent Shear Layer," *Journal of Fluid Mechanics*, Vol. 125, 1981, pp. 397-410.